Journal of
Materials Chemistry B

Accepted Manuscript

This article can be cited before page numbers have been issued, to do this please use: Z. Chen, Z. Zhang, M. Chen, S. Xie, T. Wang and X. Li, *J. Mater. Chem. B*, 2019, DOI: 10.1039/C8TB02843E.

ROYAL SOCIETY OF CHEMISTRY

rsc.li/materials-b

View Article Online
DOI: 10.1039/C8TB02843E

Journal Name

ARTICLE

Synergistic antitumor efficacy of hybrid micelles with mitochondrial targeting and stimuli-responsive drug release

Received 00th January 20xx,
Accepted 00th January 20xx

DOI: 10.1039/x0xx00000x

www.rsc.org/

Zhoujiang Chen,[a,b] Zhanlin Zhang,[a] Maohua Chen,[a] Songzhi Xie,[a] Tao Wang,[a] Xiaohong Li[a,*]

The term synergism means that the overall therapeutic benefits should be greater than the sum of the effects of individual agents and that the optimal therapeutic efficacy can be achieved at reduced doses. Micellar systems usually fail to deliver multiple drugs to target sites at synergistic doses and thus are not able to maximize the antitumor efficacy. In the current study, we demonstrate a strategy to coordinate the release of camptothecin (CPT) and α-tocopherylsuccinate (TOS) from hybrid micelles for nucleus and mitochondrion interferences. TOS is decorated with cationic triphenylphosphonium (TPP) to promote the targeting capability of TOS-TPP to mitochondria. The combination of CPT and TOS-TPP shows strong synergistism with a combination index of 0.186. Hyaluronic acid (HA) is conjugated with CPT or TOS-TPP *via* disulfide linkages for tumor cell targeting and intracellular reduction-triggered release. Both conjugates either separately self-assemble into M_C and M_T micelles, or are blended at different ratios to form $M_{C\text{-}T}$ hybrid micelles. In response to elevated intracellular glutathione levels, the coordinate release of CPT and TOS-TPP from $M_{C\text{-}T}$ results in a combination index of 0.26 and the dose-reduction indexes of CPT and TOS are 7.7 and 3.4, respectively. Compared with M_C and M_T, $M_{C\text{-}T}$ micelles with 5 folds lower doses produce higher intracellular reactive oxygen species (ROS) levels, comparable tumor growth inhibitions and animal survivals while indicating no hematologic and intestinal toxicities. Moreover, HA conjugates of $M_{C\text{-}T}$ are linked with polylactide *via* acid-labile linkages and electrospun into short fibers ($M_{C\text{-}T}$@SF) as an injectable depot to release $M_{C\text{-}T}$ in response to the acidic tumor microenvironment. At the predetermined synergistic ratio, $M_{C\text{-}T}$@SF with 5 folds lower doses achieve antitumor profiles comparable to those of individual micelles-loaded short fibers. Therefore, the hybrid micelles and micelles-releasing short fibers represent a feasible strategy to synergistically enhance the therapeutic efficacy and enable significant reductions in effective doses of chemotherapeutic agents.

1. Introduction

Cancer therapy is confronted with great challenges in improving therapeutic efficacy while alleviating systemic toxicity. Drug combinations have become a standard regimen in clinical practice to treat multi-factorial diseases and address the limitations of single-drug therapy.[1] Drugs that are typically used in combination act through different therapeutic mechanisms to produce complementary and synergistic effects, thus strengthening the treatment outcome.[2] In addition, liposomes, nanoparticles and micelles have been developed to enhance drug accumulation in tumors and retard the drug resistance. Micelles self-assembled from amphiphilic copolymers are in general more stable than liposomes and emulsions constructed from conventional surfactants, and the self-assembling structure leads to higher stimuli-responsiveness than nanoparticles.[3] The hydrophobic inner core of a micelle contributes to high loadings of poorly water-soluble drugs, while the hydrophilic outer shell as well as their nanoscale dimensions can reduce reticuloendothelial system clearances and increase tumor-specific accumulations.[4] Moreover, stimuli-responsiveness has been incorporated into micelles to release the payload in response to certain triggers like pH, light, redox potentials or tumor-specific proteases.[5]

Recently micelles have shown considerable promise as multidrug delivery carriers for enhancing tumor accumulation and synergism between anticancer drugs.[6] Kutty *et al.* fabricated micelles for the co-delivery of suberoylanilide hydroxamic acid and paclitaxel, leading to significantly higher cytotoxicities than the mere combination of free drugs.[7] However, it is still considered rather challenging to simultaneously load multiple drugs at an optimal dose ratio and achieve controlled release at the targeted sites for a synergistic efficacy, owing to the differences in the hydrophilic and pharmacokinetic properties of individual drugs.[8] For instance, paclitaxel and doxorubicin were co-loaded into recombinant high-density lipoprotein nanoparticles at the

[a] Key Laboratory of Advanced Technologies of Materials, Ministry of Education, School of Materials Science and Engineering, Southwest Jiaotong University, Chengdu 610031, P.R. China. E-mail: xhli@swjtu.edu.cn; Fax: +86 28-87634649; Tel: +86 28-87634068
[b] College of Chemical Engineering, Huaqiao University, Xiamen 361021, P.R. China.

Electronic Supplementary Information (ESI) available: The preparation of TOS-TPP, HA-ss-TOS-TPP, PLA-cdm-M_C and PLA-cdm-M_T; the CMC determination and cellular uptake images of hybrid micelles, the ROS production and cell apoptosis, typical H&E and IHC staining images of tumors and systemic toxicities after micelle treatment; the characterization and micelles release from short fibers, typical H&E and IHC staining images of tumors retrieved after short fiber treatment are included in the Supporting Information. See DOI: 10.1039/x0xx00000x

designed ratios for efficacious combination chemotherapy, but their release rates were quite diverse and the leakage of physically encapsulated drugs during blood circulation was inevitable.[9] To minimize the premature drug release during blood circulation, camptothecin and doxorubicin were covalently conjugated to polymers and released by hydrolysis of ester and amide bonds, and the different drug release rates affected the treatment efficacy of the combination.[10] It should be noted that the term synergistic effect means that the overall therapeutic benefits of micelle combinations are much greater than the sum of the effects of individual micelles, and that the therapeutic efficacy can be achieved at reduced doses.[11] Though the above reports demonstrated that multi-drug loaded micelles significantly improved the therapeutic efficacy compared to individual-drug loaded ones, few studies have confirmed the synergistic effect of micelles and enabled significant reductions in effective doses of chemotherapeutic agents. Therefore, it remains great challenges for the micellar system to achieve a synergistic dose by synchronizing the drug loading, blood circulation, cellular uptake and intracellular release in target tumor cells.

Another challenge for micellar system is the limited drug accumulation in tumors after intravenous administration. Up to now few micelles have progressed through clinical trials, mainly due to their removal from the blood compartment and premature drug release in the systemic circulation.[12] Localized chemotherapy is an effective means to maintain therapeutic levels of anticancer agents at the tumor site and relieve systemic toxicities.[13] The intratumoral injection of hydrogels is initially used to locally deliver free drugs and nanoparticles, but suffers from extensive burst release after injection into tumors, due to the lag time between the injection and precipitation/gelation process.[14] Electrospun fibers represent a superior alternative for localized chemotherapy, due to the extremely large surface area, high porosity, and great flexibility in matrix polymer selection.[15] Previously, we constructed an injectable and biodegradable short fibers for local and sustained release of micelles in response to tumor pH, enhancing drug accumulation and retention in tumor tissues.[16]

In the current study, camptothecin (CPT) and α-tocopherylsuccinate (TOS) are combined into hybrid micelles to interfere with nuclear and mitochondrial functions, respectively. CPT is an inhibitor of the nuclear enzyme topoisomerase-I and TOS is one of the most important agents to trigger mitochondrial apoptosis. Their combination is supposed to improve cancer treatment efficacy, as mitochondria maintain a central role in cellular homeostasis, energy production and apoptosis managing.[17] In addition, mitochondria show an excessively negative potential (-160 to -180 mV) across the inner membrane,[17] thus TOS is decorated with cationic triphenylphosphonium (TPP) to promote the mitochondrial targeting ability of TOS-TPP. To alleviate premature drug release before cellular internalization of micelles, CPT or TOS-TPP is conjugated to hyaluronic acid (HA) *via* disulfide linkages. Both conjugates are mixed to prepare M_{C-T} hybrid micelles (Scheme 1a). After defining the synergistic ratios of M_C and M_T, HA conjugates of M_{C-T} are linked with poly(DL-lactide) (PLA) *via* 2-propionic-3-methylmaleic anhydride (CDM) linkages to obtain PLA-cdm-M_{C-T}, followed by configuration into short fibers for intratumoral injection. As shown in Scheme 1b, in response to the acidic microenvironment of tumors,[18] the acid-labile degradation of fiber matrices leads to the release of HA conjugates and simultaneous self-assembly into M_{C-T}. In response to elevated glutathione (GSH) levels in tumor cells,[19] M_{C-T} micelles release free drugs after HA-mediated cell internalization. The synchronous breakage of disulfide linkages leads to coordinated release of CPT and TOS-TPP at the predetermined synergistic ratio. Thus, hybrid micelle-releasing short fibers can overcome barriers in the drug delivery pathway to tumor cells and the synergistic drug combinations can improve the therapeutic efficacy with dose-reducing superiority.

2. Experimental

2.1 Materials

HA (*M*w: 9.8 kDa) was purchased from the Freda Biochem Co., Ltd. (Shandong, China), and CPT was from Knowshine Pharmachemicals Inc. (Shanghai, China). Cystamine, lysine, TOS, TPP and GSH were used as received from Aladdin (Beijing, China). Triton X-100, propidium iodide, trypsin, pyrene, 3-(4,5-dimethylthiazol-2-yl)-2,5-diphenyltetrazolium bromide (MTT), 2,7-dichlorodihydrofluorescein diacetate (DCFH-DA), and dialysis bags were procured from Sigma (St. Louis, MO). Rabbit anti-mouse antibodies of caspase-3 and Ki-67, goat anti-rabbit IgG–horseradish peroxidase (HRP) and 3,3′-diaminobenzidine (DAB) developer were purchased from Biosynthesis Biotechnology Co., Ltd. (Beijing, China). All other chemicals were of analytical grade and obtained from Changzheng Regents Company (Chengdu, China), unless otherwise indicated.

2.2 Preparation and characterization of hybrid micelles

TOS-TPP was synthesized by coupling of TOS with TPP-COOH via lysine linkers, and CPT and TOS-TPP were conjugated with HA using cystamine as disulfide linkers to obtain HA-ss-CPT and HA-ss-TOS-TPP, respectively (Scheme S1). The preparation and characterizaiton results are included in the Supporting Information. Blends of HA-ss-CPT with HA-ss-TOS-TPP self-assembled into M_{C-T} via ultrasonication as described previously.[20] Briefly, different mass ratios of HA-ss-TOS-TPP and HA-ss-CPT were dispersed in distilled water with a total concentration 1 mg/mL, followed by sonication for 10 min using a probe-type ultrasonicator. The resulting micelles were filtrated through 0.45 μm pore-sized membranes. Similarly, HA-ss-CPT and HA-ss-TOS-TPP were used to prepare M_C and M_T micelles, respectively. The micelle size and zeta potential were measured by dynamic light scattering (DLS, Nano-ZS90, Malvern Ltd., UK). The morphology was observed by transmission electron microscopy (TEM, Tecnai G2 F20 S-Twin, FEI, USA). The critical micellar concentrations (CMCs) of M_C and M_T micelles were determined by fluorescence spectroscopy using a pyrene probe as described previously.[21]

View Article Online
DOI: 10.1039/C8TB02843E

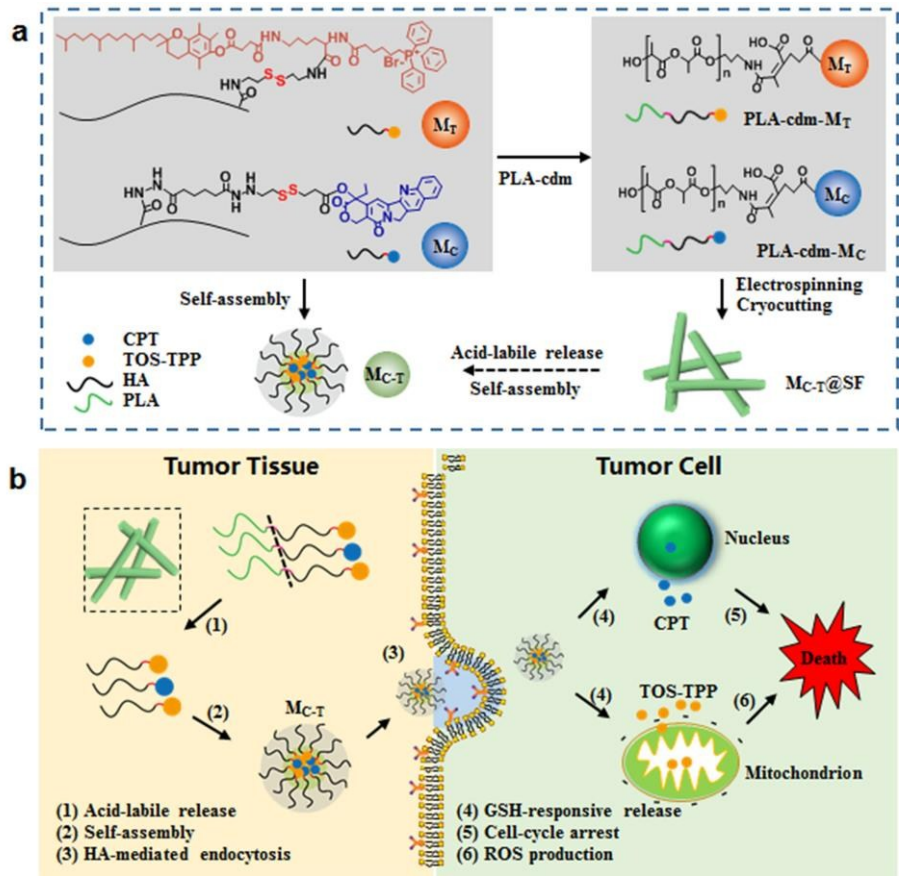

Scheme 1. (a) Synthesis routes of PLA-cdm-M_T and PLA-cdm-M_C copolymers by conjugation of M_T and M_C carriers with PLA-cdm. M_T and M_C self-assemble into $M_{C\text{-}T}$ hybrid micelles, and PLA-cdm-M_T and PLA-cdm-M_C are blended and configured into $M_{C\text{-}T}$@SF short fibers. (b) Schematic drawing of the release of HA-drug conjugates from short fibers in response to the slightly acidic tumor matrix (1), followed by self-assembly into hybrid micelles (2); The hybrid micelles are endocytosed into tumor cells via HA mediation (3); In response to intracellular GSH, CPT and TOS-TPP are released to target nuclei and mitochondria (4) for induction of cell-cycle arrest (5) and reactive oxygen species (ROS) production (6).

2.3 Preparation and characterization of short fibers with loaded hybrid micelles

Micelle carriers of M_C and M_T were conjugated with PLA via acid-labile CDM linkers to obtain PLA-cdm-M_C and PLA-cdm-M_T copolymers (Scheme 1a), and the preparation and characterizaiton results are included in the Supporting Information. PLA-cdm-M_C, PLA-cdm-M_T and their blends with the weight ratio of 1/2 were used to prepare injectable short fibers (M_C@SF, M_T@SF and $M_{C\text{-}T}$@SF).[16] Briefly, the matrix polymers were dissolved in chloroform/dimethyl formamide (5/1, v/v), and electrospun fibers were deposited on a grounded rotating mandrel. Aligned fibers were cryosectioned with a thickness of 20 μm, followed by ultrasonication of the fiber bundles to harvest short fibers. The morphology of short fibers were detected by scanning electron microscopy (SEM; FEI Quanta 200, The Netherlands) equipped with a field-emission gun (20 kV) and a Robinson detector after 2 min of gold coating to minimize the charging effect. The diameter and length of short fibers were measured from SEM images to generate an average value by using the tool of Photoshop 10.0 edition.

The degradation and micelle release from short fibers were determined after incubation in pH 7.4 and pH 6.8 buffers as described previously.[16] Briefly, short fibers (around 20 mg) were exactly weighed and placed into dialysis bags (3.5 kDa cut off) and immersed into 30 ml of release media at 37 °C. At predetermined time intervals, short fibers were retrieved for weight loss measurement. The molecular weight of matrix polymers was detected by gel permeation chromatography (GPC, Waters 2695 and 2414, Milford, MA) using polystyrene as standard. The molecular structure was determined by nuclear magnetic resonance (NMR) spectroscopy (Bruker AM 400 apparatus). In addition, 1.0 mL of the released media was withdrawn from inside and outside the dialysis bag for analysis of the released micelles and free drugs respectively, and equal amount of fresh buffers was added back. The micelle and drug concentrations were detected by a fluorescence spectrophotometer (Hitachi F-7000, Japan) at the excitation/emission wavelengths of 298/345 and 365/430 nm for M_T (or TOS-TPP) and M_C (or CPT), respectively. In another batch of experiment, $M_{C\text{-}T}$@SF short fibers were incubated in pH 6.8 buffers for 3 days and the released micelles were

retrieved for morphological observation and reductive sensitivity determination.

2.4 Reductive sensitivity of hybrid micelles

The reductive sensitivity of micelles (M_C, M_T, and $M_{C\text{-}T}$) and the retrieved micelles after release from short fibers was measured from the size change and drug release profiles in response to 10 μM and 10 and 40 mM GSH in PBS. Briefly, micelle suspensions were placed in dialysis bags (1 kDa cutoff), which were immersed into 30 mL of release media to achieve a sink condition and kept shaking at 37 °C. After incubation for 48 h, micelles were retrieved and the size changes were monitored by DLS as above. At given time intervals, 1 mL of release media were withdrawn and refreshed with PBS containing GSH. The TOS-TPP and CPT in the retreived media were detected by a fluorospectrophotometer as above.

2.5 Cellular uptake of hybrid micelles

The cellular uptake of M_C, M_T, and $M_{C\text{-}T}$ micelles was evaluated on H22 cells as described previously.[21] Briefly, H22 cells from the American Type Culture Collection (Rockville, MD) were cultured in RPMI 1640 (Invitrogen, Grand Island NY) supplemented with 10% heat inactivated fetal bovine serum (FBS, Gibco BRL, Grand Island, NY). H22 cells were seeded into 6-well tissue culture plates (TCPs) at a density of 1.0×10^6 cells/well and incubated for 24 h before treatment. Then the cells were cultured in media containing free drug (CPT and TOS-TPP) or micelles with a final drug concentration of 10.0 μg/mL. For comparison, media containing 5 mg/mL of HA were tested and cells without treatment were used as control. After incubation for 6 h, cells were washed with PBS, lysed by 500 μl of 0.5% Triton X-100 for 2 h at 4 °C. The fluorescence intensity of the cell lysate was detected by a fluorescence spectrophotometer as above, and the cellular uptake efficiency was obtained by comparison with the fluorescence intensity of drugs or micelles added. In another batch of experiment, H22 cells were seeded into 24-well TCP at a density of 1×10^5 cells/well. After treatment as above for 6 h, the culture media were removed, and cells were washed with PBS and fixed with 4% paraformaldehyde. The cell nuclei were stained with propidium iodide and observed by confocal laser scanning microscopy (CLSM, Leica TCS SP2, Germany).

2.6 Cytotoxicity synergism of free drugs, hybrid micelles and short fibers

The cytotoxicity of free drugs and micelles was detected by alamar Blue assay as described previously.[22] Briefly, H22 cells were seeded in 96-well TCPs at a density of 1×10^4 cells/well and incubated for 24 h. Media were then replaced with fresh media containing various concentrations of free drugs (CPT, TOS, and TOS-TPP) from 0.1 to 100 μM and micelles (M_C and M_T) from 0.01 to 10 μM, using cells without treatment as control. After treatment for 72 h, 10 μL of alamar Blue reagent (Yeasen Biological Technology Co., Shanghai, China) was added into each well, allowing to incubate at 37 °C for 1 h. The absorbance of each well was measured using a μQuant microplate spectrophotometer (Elx-800, Bio-Tek Instrument Inc., Winooski, VT). On the basis of IC50s of CPT, TOS, and TOS-TPP, the mixtures of CPT/TOS and CPT/TOS-TPP were tested at concentrations of 2 and 4 folds higher or lower than their IC50s to assess of the synergistic cytotoxicities.[23,24] In addition, $M_{C\text{-}T}$ were detected under different ratios of HA-ss-CPT to HA-ss-TOS-TPP. Based on the cell viability data after single and combination treatment, the synergism of free drugs and hybrid micelles was determined using CalcuSyn software as described previously.[25] Synergism, additivism, and antagonism were indicated by the combination indexes less than 1, equal to 1, and greater than 1, respectively.

The cytotoxicities of micelles released from short fibers were evaluated on H22 cells after incubation in pH 7.4 and 6.8 media as described previously.[16] The cell culture under pH 6.8 was performed by adjusting the pH of culture media with 0.1 M HCl.[26] The cells were treated by short fibers with the equal amount of micelles released in pH 6.8 buffers during 72 h. The cytotoxicity was determined by alamar Blue assay as above.

2.7 ROS production, cell apoptosis and cell cycle analysis

TOS is known to be able to destabilize mitochondria in tumor cells, which often involves the elevated formation and buildup of intracellular ROS.[27] The intracellar ROS levels and cell apoptosis were detected after treatment of H22 cells with free drugs (CPT, TOS, and TOS-TPP) or micelles (M_C, M_T, and $M_{C\text{-}T}$), using cells without treatment as control. Briefly, cells were cultured on 6-well TCPs at 5×10^5 cells/well, followed by exposure to micelles and free drugs at the final drug concentration of 5 μg/mL. After treatment for 6 h, cells were collected, suspended, and incubated with DCFH-DA (10 μM) at 37 °C for 20 min according to the manufacturer's protocol, followed by fluorescence measurement via flow cytometry (BD Accuri C6, Franklin Lakes, NJ).[28] In antoher batch of experiment, the adherent and non-adherent cells were collected after 48 h of incubation, suspended in the binding buffer and stained using the Annexin V-FITC apoptosis detection kit (Beijing 4A Biotech Co., Beijing, China).[29]

2.8 *In vivo* antitumor efficacy of hybrid micelles and short fibers

All animal procedures were performed in accordance with the National Institutes of Health Guide for Care and Use of Laboratory Animals of China and approved by the Animal Care and Use Committee of Southwest Jiaotong University. The antitumor efficacy was determined from the tumor growth inhibition, animal survival and histological analysis of tumors retrieved as described previously.[16] Briefly, female Kunming mice weighing 22 ± 2 g were supplied by Sichuan Dashuo Biotech Inc. (Chengdu, China). H22 cells were maintained in the peritoneal cavities of mice for around 1 week, and the ascites was withdrawn and diluted with PBS at $l \times 10^7$ cells/mL. The cell suspension was subcutaneously inoculated into the right armpit region of each animal at a dose of 5×10^6 cells per mouse, allowing the tumor growth to 50–100 mm^3. The established tumor-bearing mice were randomly divided into eight groups with 8 mice per group. Free drugs (CPT and TOS)

and micelles (M_C, M_T, and $M_{C\text{-}T}$) at equivalent doses of 4 mg CPT/kg and 8 mg TOS/kg were injected through the tail vein on days 0, 2, 4, and 6, using saline injection as control. $M_{C\text{-}T}$ hybrid micelles with dilutions of 5 and 10 folds were also tested and defined as $M_{C\text{-}T}$(1/5), and $M_{C\text{-}T}$(1/10), respectively. In another batch of experiment, when tumors reached about 500 mm^3 in volume after 10 days of growth, the tumor-bearing mice were randomly divided into five groups with 8 mice per group. The mice were intratumorally injected with M_C@SF, M_T@SF and $M_{C\text{-}T}$@SF at equivalent doses of 4 mg CPT/kg and 8 mg TOS/kg, using PBS as control. The 5-flod lower dose of short fibers were also tested and named as $M_{C\text{-}T}$@SF(1/5).

The body weights, tumor volumes and survival rates of mice were measured every two days after treatment. To calculate the tumor volume, the lengths of the major axis (longest diameter) and minor axis (perpendicular to the major axis) of a tumor were measured with a vernier caliper.[16] Survival curves were plotted at each time point, and the treatment efficacy was evaluated according to the 50% mean survival time. After treatment for 21 days, mice were sacrificed to remove tumors, followed by embedding in paraffin and cutting with a microtome at a thickness of 4 μm. Tumor sections were stained with hematoxylin and eosin (H&E) to evaluate the cell morphology and tissue necrosis. Immunohistochemical (IHC) staining of Ki-67 and caspase-3 was performed on tumor sections for investigating the proliferation and apoptosis. The slides were observed with a light microscope (Nikon Eclipse E400, Japan) and the positively stained cells of Ki-67 or caspase-3 were counted in five randomly areas in IHC staining images. The ratios of proliferation or apoptosis were obtained by comparing with the total number of cells in the same areas.

2.9 Systemic toxicity of hybrid micelle treatment

Except the body weight, the blood and intestinal toxicity are important indicators for examining the toxicity of CPT. Mice of each group were randomly chosen and sacrificed on day 21 after treatment. Blood was taken from the eyes, and white blood cells (WBC), red blood cells (RBC) and lymphocytes were counted by an auto hematology analyzer (TEK-II MINI, Tecom Science Co., China). The jejunums were removed and washed with PBS, fixed in 4% formaldehyde, embedded in paraffin, and cut into sections for H&E staining.

2.10 Statistical analysis

Data are expressed as mean ± standard deviation. Whenever appropriate, comparisons among multiple groups were performed by analysis of variance, while a two-tailed Student's *t*-test was used to discern the statistical difference between two groups. A probability value (p) of less than 0.05 was considered to be statistically significant.

3. Results and discussion

3.1 Synergistic effect of CPT and TOS-TPP

Owing to the large potential from -160 to -180 mV across mitochondrial membrane,[17] TOS was modified with cationic TPP moieties to increase the target delivery to mitochondria. Gogvadze *et al.* indicated that vitamin E analog was 20–50 folds more efficient in mitochondrial targeting than TOS.[30] As shown in Scheme S1a, TPP containing a single amino group was synthesized *via* sequential reaction with 6-bromohexanoic acid and lysine and then coupled with TOS by DCC/NHS chemistry to obtain TOS-TPP (Fig. S1).

The combination index analysis is an effective way to determine optimal drug combinations that work synergistically.[11,31] Fig. 1a shows the cytotoxicities of CPT, TOS, and TOS-TPP against H22 cells with IC_{50} values of about 1.19, 3.14 and 0.99 μg/mL, respectively. TOS-TPP possessed higher cytotoxicity, since the positive charge of TPP enhanced the cellular uptake and mitochondrial targeting. The cytotoxic activities of TOS or TOS-TPP used in combination with CPT were determined at 0.25, 0.5, 1, 2 and 4 folds of their IC_{50} concentrations.[23,24] As shown in Fig. 1b, both combinations exhibited strong growth inhibition at low drug concentrations. The combination index of TOS and CPT was 0.238, while that of TOS-TPP and CPT was 0.186. Both combinations showed strong synergism by combination indexes below 0.3.[32] The combination of CPT with TOS-TPP exhibited higher synergistic effect, suggesting that the conjugation of TPP to TOS not only enhanced the cytotoxicity of TOS, but also improved the combined effect with CPT.

3.2 Characterization of hybrid micelles

Cystamine was conjugated onto HA to introduce disulfide linkages and terminal amino groups, followed by TOS-TPP coupling *via* a condensation reacton. The substitution degree of cystamine on HA was around 30%, which was defined as the number of cystamine molecules per 100 sugar residues of HA. The substitution degree of TOS-TPP on HA was 15.1%, and the drug loading was aroud 13.0% as determined from the ^{1}H-NMR spectrum (Fig. S2). HA-ss-TOS-TPP copolymers were self-assembled into M_T micelles with an average hydrodynamic diameter of 98 nm, while M_C micelles had an average size of around 160 nm (Fig. 1c). As shown in Fig. S4, the CMCs of M_T and M_C micelles were around 2.7 and 3.1 μg/mL. Fig. 1d shows the size and zeta potential of $M_{C\text{-}T}$ hybrid micelles self-assembled from blends of HA-ss-CPT and HA-ss-TOS-TPP with different ratios. The avergage size of $M_{C\text{-}T}$ micelles gradually decreased with increasing HA-ss-TOS-TPP contents in the mixtures. In addition, the DLS analysis revealed a single peak, suggesting that $M_{C\text{-}T}$ micelles were in a hybrid not a mixed state. Fig. 1e shows TEM images of M_T and $M_{C\text{-}T}$ micelles, displaying spherical morphologies with average sizes of 46 and 58 nm, respectively.

3.3 Reductive sensitivity of hybrid micelles

The reductive sensitivities of micelles were monitored with respect to the varations in size and drug release after incubation in PBS containing 10 μM and 10 and 40 mM GSH. As shown in Fig. 2a, the average sizes of M_C, M_T, and $M_{C\text{-}T}$ micelles were around 167, 98, and 126 nm, respectively, after

View Article Online
DOI: 10.1039/C8TB02843E

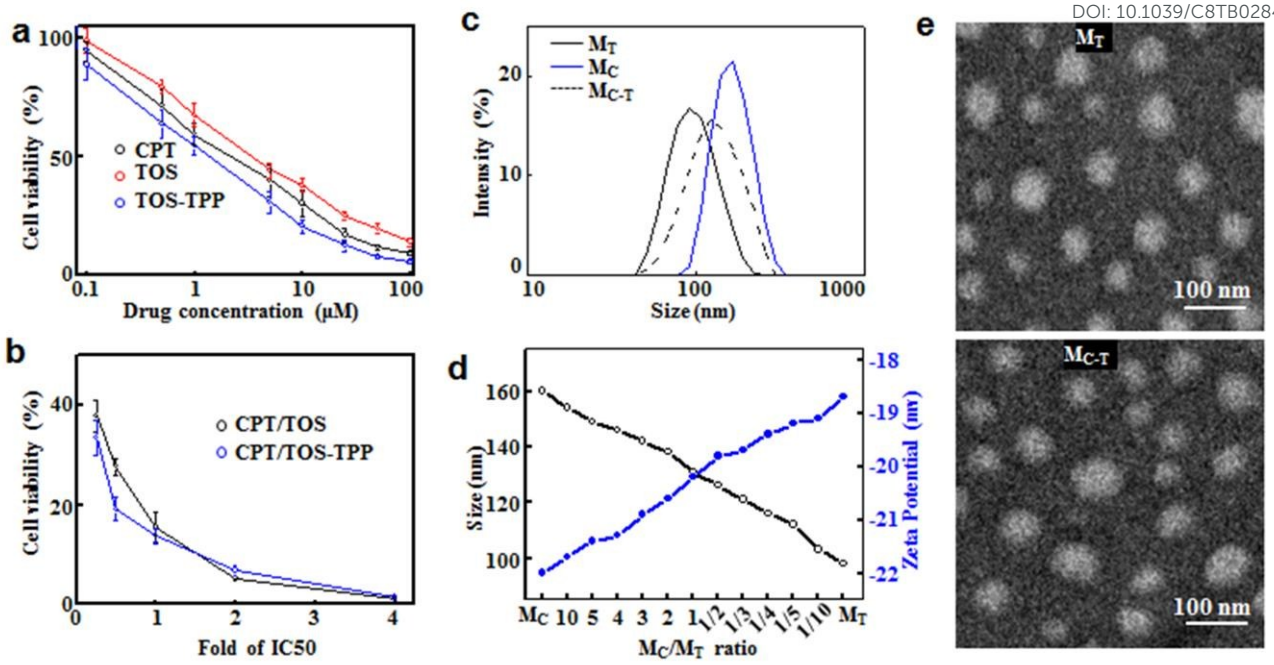

Fig. 1. Characterization of synergistic cytotoxicities of CPT and TOS-TPP and the formation of hybrid micelles (n = 3). (a) Cytotoxicity to H22 cells after incubation for 72 h with CPT, TOS and TOS-TPP. (b) Cytotoxicity of CPT combined with TOS or TOS-TPP at 0.25, 0.5, 1, 2 and 4 folds of their IC50 concentrations. (c) Size distributions of M_T, M_C, and M_{C-T} micelles (M_C/M_T ratio: 1/2) determined by DLS measurement. (d) Average sizes and zeta potentials of hybrid micelles with different ratios of M_C and M_T. (e) Typical TEM images of M_T and M_{C-T} micelles.

incubation at the plasma GSH level (*i.e.* 10 μM), indicating no significant difference from those of prinstine micelles (Fig. 1c). In contrast, M_C, M_T, and M_{C-T} micelles indicated rapid size increases to around 985, 451 and 586 nm, respectively, after incubation with 40 mM GSH, corresponding to the GSH concentration in cytoplasma of tumor cells.[33] It was indicated that the micelles disintegrated once internalized into tumor cells.

Fig. 2b,c summarizes the drug release behaviors of M_C and M_T micelles, indicating simialr profiles in response to GSH concentrations. Around 6% of drugs were relased from micelles after 24 h of incubation with 10 μM GSH. The drug release from micelles was remarkably accelerated in the presence of 10 and 40 mM GSH due to thiol-disulfide exchange reactions. For instance, about 13.6% of TOS-TPP was released from M_T micelles in 4 h and near 46.5% in 24 h after incubation with 10 mM GSH. As shown in Fig. 2d, there were around 60% of CPT and TOS-TPP released from M_{C-T} after 24 h of incubation with 40 mM GSH, while less than 5% in PBS, indicaitng redox-dependent drug release like M_C and M_T. The release of CPT or TOS-TPP from M_{C-T} showed a similar profile, thus, the ratios of HA-ss-CPT and HA-ss-TOS-TPP used for hybrid micelle preparation should represent the drug ratios after the GSH-responsive release. In addition, the thiolated compounds released after the breakage of disulfide linkages indicated cytotoxicities and cytotoxic mechanisms similar to those of free drugs.[34] Therefore, the synchronous release of TOS-TPP and CPT from M_{C-T} was beneficial to control the ratio of drugs reaching the cell nuclei and mitochondria.

3.4 Synergistic cytotoxicity of hybrid micelles

M_C and M_T micelles had IC_{50} values of 0.92 and 0.73 μg/mL against H22 cells (Fig. 3a). M_{C-T} hybrid micelles self-assembled from HA-ss-CPT and HA-ss-TOS-TPP with different ratios showed dose-dependent growth-inhibitory effect (Fig. 3b). Fig. 3c summarizes combination indexes of M_{C-T} at different molar ratios of HA-ss-CPT and HA-ss-TOS-TPP. The lowest combination index was 0.26 at the M_c/M_T ratio of 1/2, which was used in the following study. In addition, the dose-reduction index is a measure of the dose for each drug alone at a given effect level compared with the dose of each drug in a synergistic combination.[35] In clinical situations the dose reduction alleviated the side effects while retaining the therapeutic efficacy. Fig. 3d shows dose-reduction indexes for various molar ratios of CPT and TOS-TPP. At the synergistic ratio of CPT to TOS-TPP at 1/2, the dose-reduction indexes of CPT and TOS-TPP were 7.7 and 3.4, respectively.

The cellular uptake of micelles was determined on H22 cells from the intracellular CPT and TOS contents after cell lysis. As shown in Fig. 3e, the cell uptake efficiency was around 34.9% and 36.7% for M_C and M_T micelles, respectively. After incubation with M_{C-T}, the uptake efficiency of CPT is about 35.2%, similar to that of TOS at about 35.0%. The addition of free HA into the culture media led to over 3-fold decrease in the uptake efficiency to around 10% ($p < 0.05$), due to competitive blocking of the receptors.[36] In addition, the uptake efficiency of free drug (CPT or TOS) was around 11%, and the increased uptake efficiency of micelles indicated that the

View Article Online
DOI: 10.1039/C8TB02843E

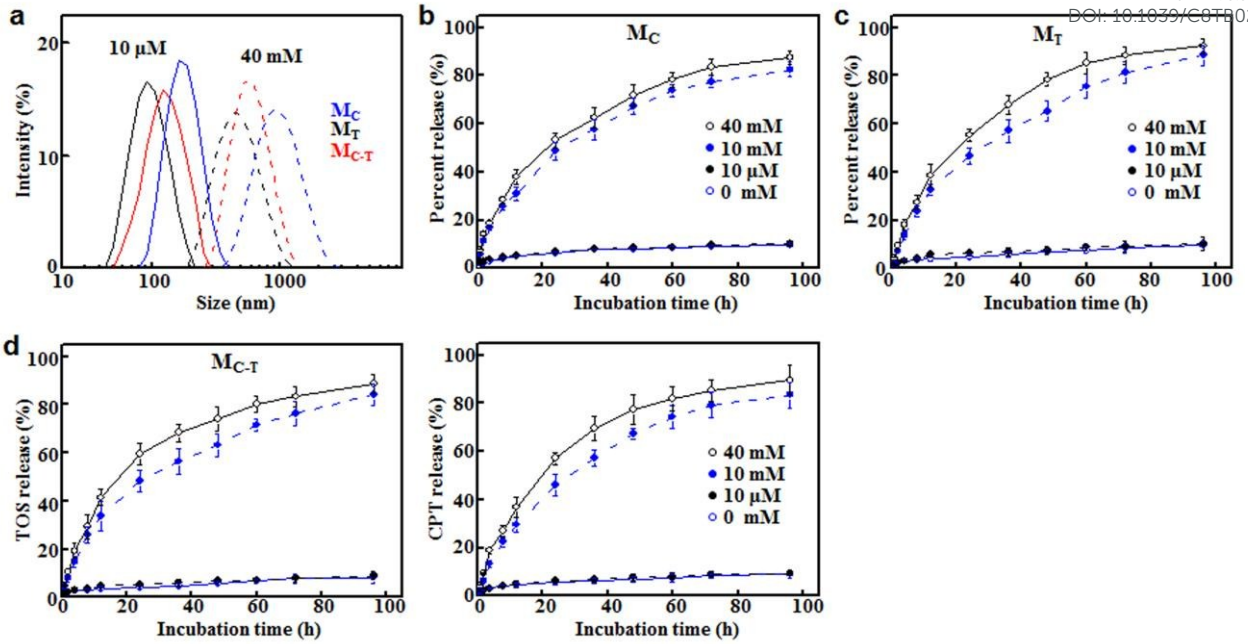

Fig. 2. Characterization of GSH responsiveness of $M_{C\text{-}T}$ hybrid micelles with M_C/M_T ratio of 1/2 (n = 3). (a) Typical DLS images of $M_{C\text{-}T}$, M_T and M_C micelles after incubation at 37 °C in PBS and PBS containing 10 μM and 40 mM GSH for 48 h. (b) Percent drug release from M_C, and (c) M_T micelles after incubation with different GSH concentrations. (d) Percent release of TOS-TPP and CPT from $M_{C\text{-}T}$ hybrid micelles after incubation with different GSH concentrations.

micelles would be good nanocarriers for combinational drug delivery. Fig. S5 shows CLSM images of H22 cells after incubaiton with M_C and $M_{C\text{-}T}$ micelles, indicating similar uptake profiles. The internalization of M_C was more effective than that of free CPT due to the CD44 receptor-mediated endocytosis. The addition of HA interfered the endocytosis of M_C but did not affect the internalization of free CPT.

Mitochondrial ROS production is an important mechanism of the mitocan-induced activation of cancer cell apoptosis.[37] The intracellular ROS levels were detected on H22 cells after treatment with micelles (M_C, M_T and $M_{C\text{-}T}$) and free drug (CPT and TOS), as well as the reduced micelle doses ($M_{C\text{-}T}$(1/5) and $M_{C\text{-}T}$(1/10)). Fig. S6 shows the flow cytometry analysis of DCF fluorescence, and Fig. 3f summarizes the ROS levels after each treatment. CPT slightly increased ROS production at 158% higher than that of controls ($p < 0.05$), due to inhibition of oxygen consumption and ROS formation in cells.[38] TOS was subjected to interfere with the ubiquinone-binding site of the mitochondrial complex II impairing electron transfer flowing along the redox chain.[39] The TOS treatment resulted in 2.7 folds higher ROS levels than controls ($p < 0.05$). The HA-mediated cellular uptake and GSH-responsive release from M_C and M_T micelles caused 1.4 and 2.2 folds higher levels than those of CPT and TOS, respectively ($p < 0.05$). As shown in Fig. 3f, $M_{C\text{-}T}$ induced significantly higher ROS levels than M_T, even $M_{C\text{-}T}$(1/5) showed stronger ROS production than M_T micelles and free drugs ($p < 0.05$).

The apoptosis induction by micelles was determined by flow cytometry after Annexin V-FITC and propidium iodide staining. Fig. S7 shows flow cytometry images of tumor cells and Fig. 3g summarizes the percentage of cells in the early and late apoptosis stages after treatment with free drug and micelles. $M_{C\text{-}T}$ induced the highest cell apoptosis of 83.4%, and the treatment with $M_{C\text{-}T}$(1/5) led to about 54.1% of apoptosis rate, which was close to those of M_C (57.8%) and M_T micelles (61.6%).

3.5 *In vivo* antitumor efficacy of hybrid micelles

The *in vivo* antitumor performance of micelles was investigated from the tumor growth inhibition, animal survival, histological and IHC staining of retrieved tumors. Fig. 4a shows the tumor growth status since the first administration of free drugs and micelles, using saline treatment as a control. Mice in the control group showed a significant increase in tumor volume to around 3320 mm^3 after 21 days. The CPT and TOS treatment indicated around 40% and 32% of tumor growth inhibition, respectively. The inhibition of M_C and M_T micelles on the tumor progressing was significantly stronger than the corresponding free drugs. Among the testing groups, $M_{C\text{-}T}$ showed the superior tumor inhibition (86%) after 21 days of treatment ($p < 0.05$). $M_{C\text{-}T}$(1/5) showed an apparent anticancer effect (around 1160 mm^3), which was close to those of M_T and Mc treatment (around 1100 mm^3). Fig. 4b summarizes the survival rates of tumor-bearing mice in a Kaplan–Meier plotting. The median survival time was 17, 22 and 23 days after treatment with PBS, free CPT and TOS. The M_C and M_T treatment prolonged animal survivals, and $M_{C\text{-}T}$ treatment displayed an extended median survival time of 34 days. In addition, 50% of mice survived after treatment with $M_{C\text{-}T}$(1/5)

View Article Online
DOI: 10.1039/C8TB02843E

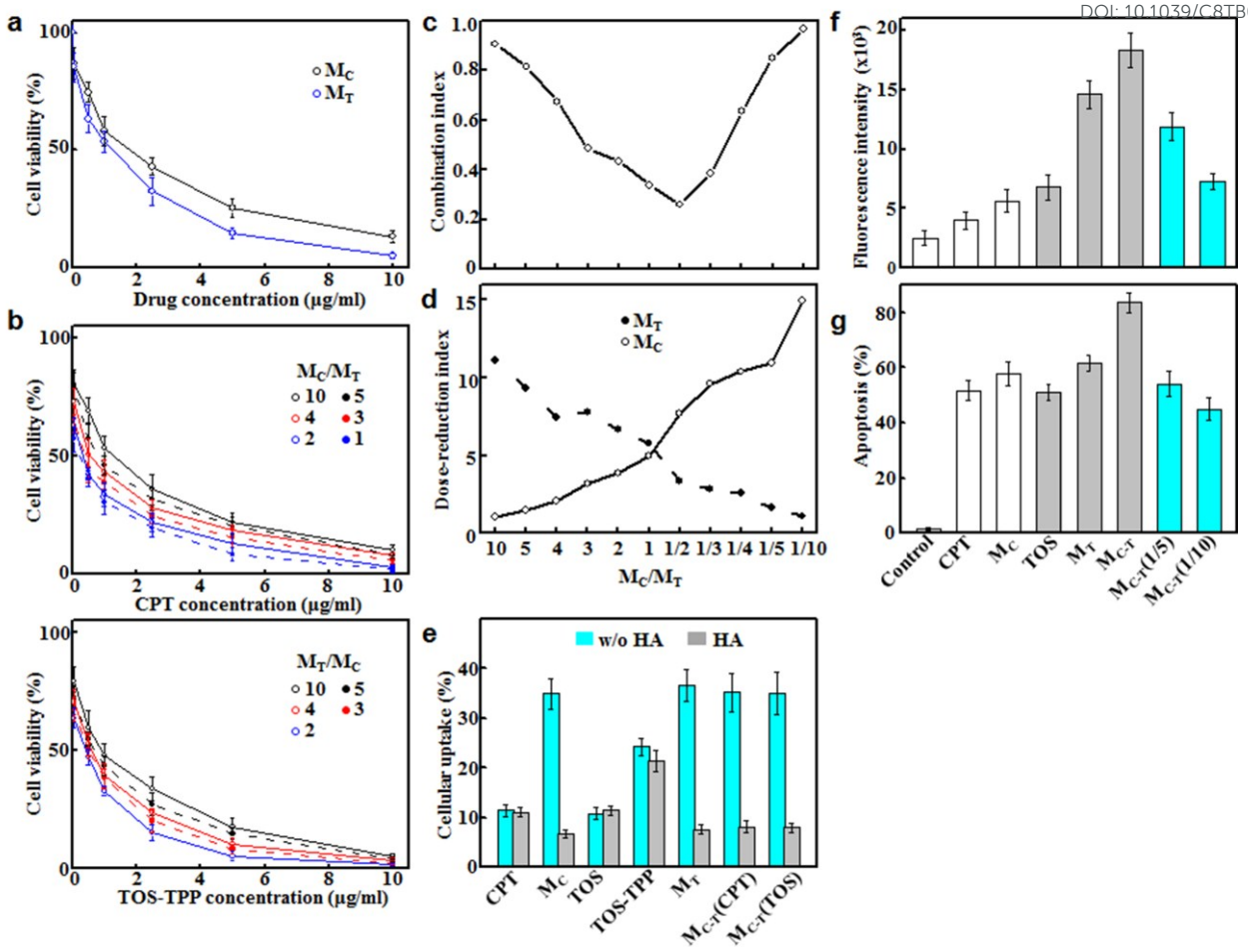

Fig. 3. Characterization of synergistic cytotoxicities of hybrid micelles (n = 3). (a) Cytotoxicity to H22 cells after incubation for 72 h with M_C and M_T. (b) Cytotoxicities, (c) combination indexes and (d) dose-reduction indexes of hybrid micelles with different ratios of M_C and M_T. (e) H22 uptake efficiency of free CPT,TOS, M_C, M_T and M_{C-T}. (f) Mean DCF fluorescent intensities in H22 cells and (g) cell apoptosis rate after incubation with PBS, free CPT, TOS, M_C, M_T, M_{C-T}, M_{C-T}(1/5) and M_{C-T}(1/10).

for 32 days, which was slightly longer than those of M_C (29 days) and M_T (30 days).

Necrosis within tumors represents a significant prognostic factor of tumor growth and survival of patients after chemotherapy.[40] As shown in Fig. 4c and Fig. S8a, H&E staining images of tumors after micelle treatments led to larger necrotic regions (pink area) than those of free drugs. A large amount of living cells (blue area) were detected in tumors in the control group, and tumor cells showed obvious nucleolus cleavage and high extent of malignancy. It should be noted that the M_{C-T}(1/5) treatment showed larger area of necrosis comparable to M_C and M_T. The cell proliferation and apoptosis in tumor tissues were evaluated by IHC staining of Ki-67 and caspase-3, respectively. Fig. 4d and Fig. S8b show IHC staining images of Ki-67, a nuclear marker of active cells in the G1, G2, and S phases of the cell cycle.[41] As shown in Fig. 4f, the M_{C-T} treatment led to around 11.2% of proliferative cells in tumors, which was significantly lower than those of M_C (39.6%) and M_T (35.2%) micelles ($p < 0.05$). The caspase family plays a crucial role in the apoptosis execution, in which caspase-3 plays a central role.[42] As revealed in IHC staining images and cell counting results (Fig. 4e,f and Fig. S8c), 97.4% of cells were apoptotic after M_{C-T} treatment, which were significantly higher than others ($p < 0.05$). It should be noted that both the cell proliferation inhibition and apoptosis induction by M_{C-T}(1/5) were comparable to those by M_C and M_T ($p > 0.05$).

3.6 *In vivo* toxicity after micelle treatment

Changes in body weight are one of the safety markers in tumor chemotherapy. As shown in Fig. S9a, there was no apparent weight loss in the groups of TOS and M_T micelles due to few toxicities of TOS to normal tissue. Free CPT treatment led to greater weight reduction than M_C and M_{C-T}. There was no apparent weight loss when reducing the dose of hybrid micelles like M_{C-T}(1/5) and M_{C-T}(1/10). CPT-associated leukopenia and gastrointestinal toxicity, especially severe diarrhea, limit its clinical applicability.[43] Fig. S9b summarizes

View Article Online DOI: 10.1039/C8TB02843E

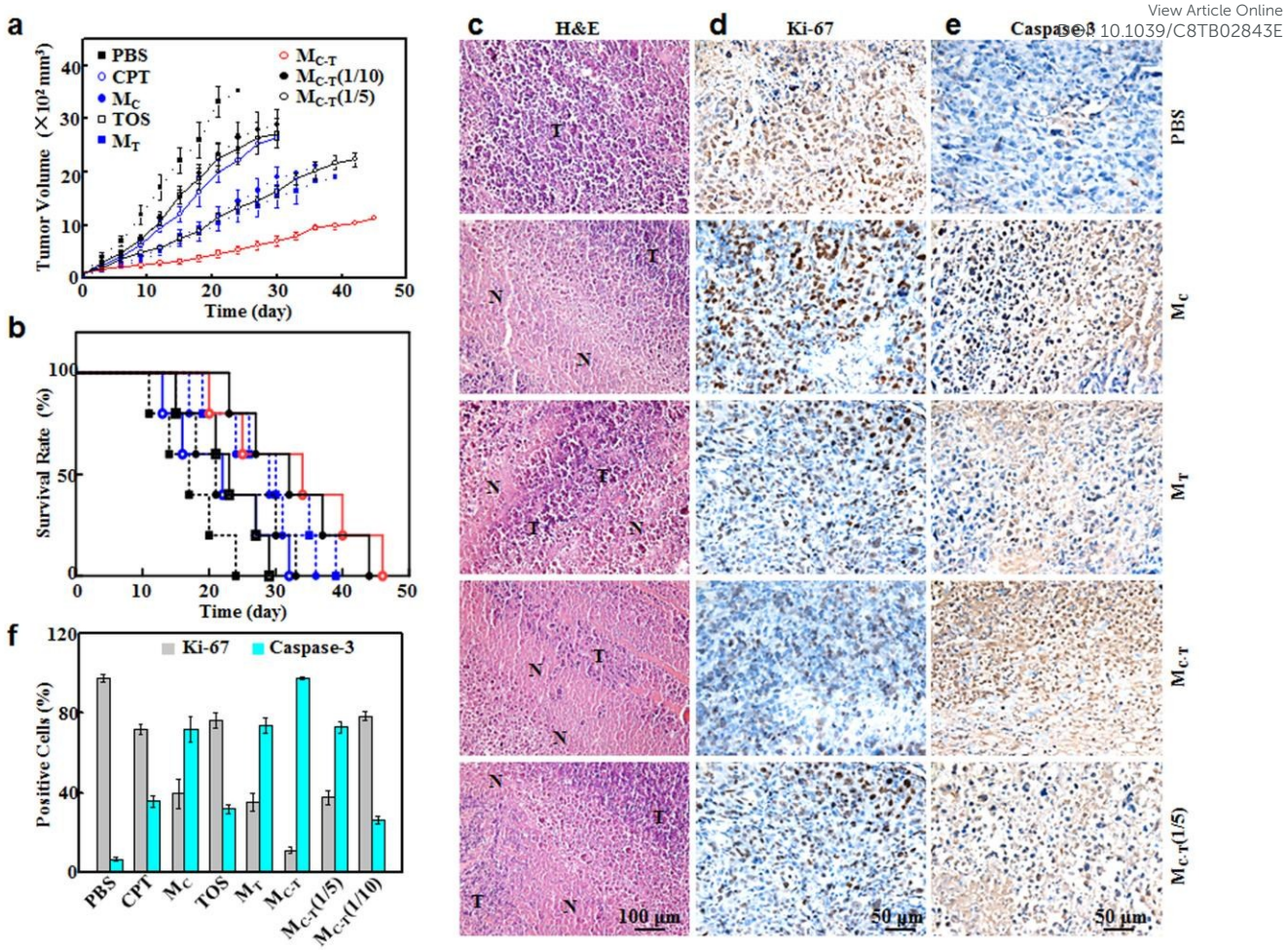

Fig. 4. *In vivo* antitumor efficacy of hybrid micelles. (a) Tumor growth, (b) overall survival of tumor-bearing mice, (c) typical H&E staining images ("N" represents necrotic area, "T" represents tumor mass), (d) IHC staining images of Ki-67 and (e) caspase-3, (f) the number of caspase-3 and Ki-67-positive cells compared with the total number of cells in IHC staining images of tumors retrieved on day 21 after intravenous administration of free CPT, TOS, M_C, M_T, M_{C-T}, M_{C-T}(1/5) and M_{C-T}(1/10), using saline injection as control (n = 8).

the numbers of WBCs, RBCs and lymphocytes in mice after treatment with free drug and micelles. Free CPT treatment showed significant decreases in the WBC and lymphocyte numbers compared with PBS, and the inoculation of CPT in M_{C-T} and M_C micelles reduced the toxicity. The lower doses of M_{C-T}(1/5) and M_{C-T}(1/10) indicated few toxicities to blood cells. The gastrointestinal toxicity was examined *via* H&E staining of small intestines retrieved after 24 h from the last injection. As shown in Fig. S9c, epithelial cells and villi were tightly arrayed in the control, M_{C-T}(1/5) and M_{C-T}(1/10) groups, but irregular villi, crypt shrink or number decrease were obviously observed after free CPT treatment. It was indicated that the micelles could reduce the toxicity of CPT, and the dose-reduced hybrid micelles showed no hematologic and intestinal toxicities.

3.7 Characterization of short fibers with loaded hybrid micelles

Scheme 1a shows the synthetic process of PLA-cdm-M_T by conjugation of HA-ss-TOS-TPP with PLA-cdm. As shown in the ^{1}H NMR spectrum of PLA-cdm-M_T (Fig. S3a), the methyl group of TOS showed a peak at 0.9 ppm, and the drug loading was about 5.4%, determined from the integral ratios of peaks at 0.9 (-CH_3) and 1.87 ppm (-CH_3) or 5.13 ppm (-CH(-C)-). GPC analysis showed that the weight-average molecular weights (Mw) of PLA-NH_2 and PLA-cdm-M_T were 26.3 and 36.8 kDa, respectively (Fig. S3c). M_C@SF, M_T@SF, and M_{C-T}@SF were obtained by electrospinning of PLA-cdm-M_C, PLA-cdm-M_T, and their blends at the weight ratio of 1/2, respectively. Fig. 5a shows typical SEM image of M_{C-T}@SF, indicating uniform morphologies with smooth surface. M_C@SF, M_T@SF, andM_{C-T}@SF showed lengths of 21.4 ± 1.3, 19.5 ± 1.1 and 20.7 ± 1.6 μm, respectively ($p > 0.05$), and the average diameter was around 1.62 ± 0.16 μm (Fig. S10a,b).

β-carboxylate amide groups show significant sensitivities to weakly acidic microenvironment in tumor tissues (*e.g.* pH 6.8),[44] thus, PLA-cdm-M_T and PLA-cdm-M_C copolymers were degraded to release micelles from short fibers. Fig. S10c shows the mass residual of M_{C-T}@SF after incubation in pH 7.4 and pH 6.8 buffers. There was a quick mass loss (around 30%) during the initial 2 weeks of incubation in pH 6.8 buffers, while

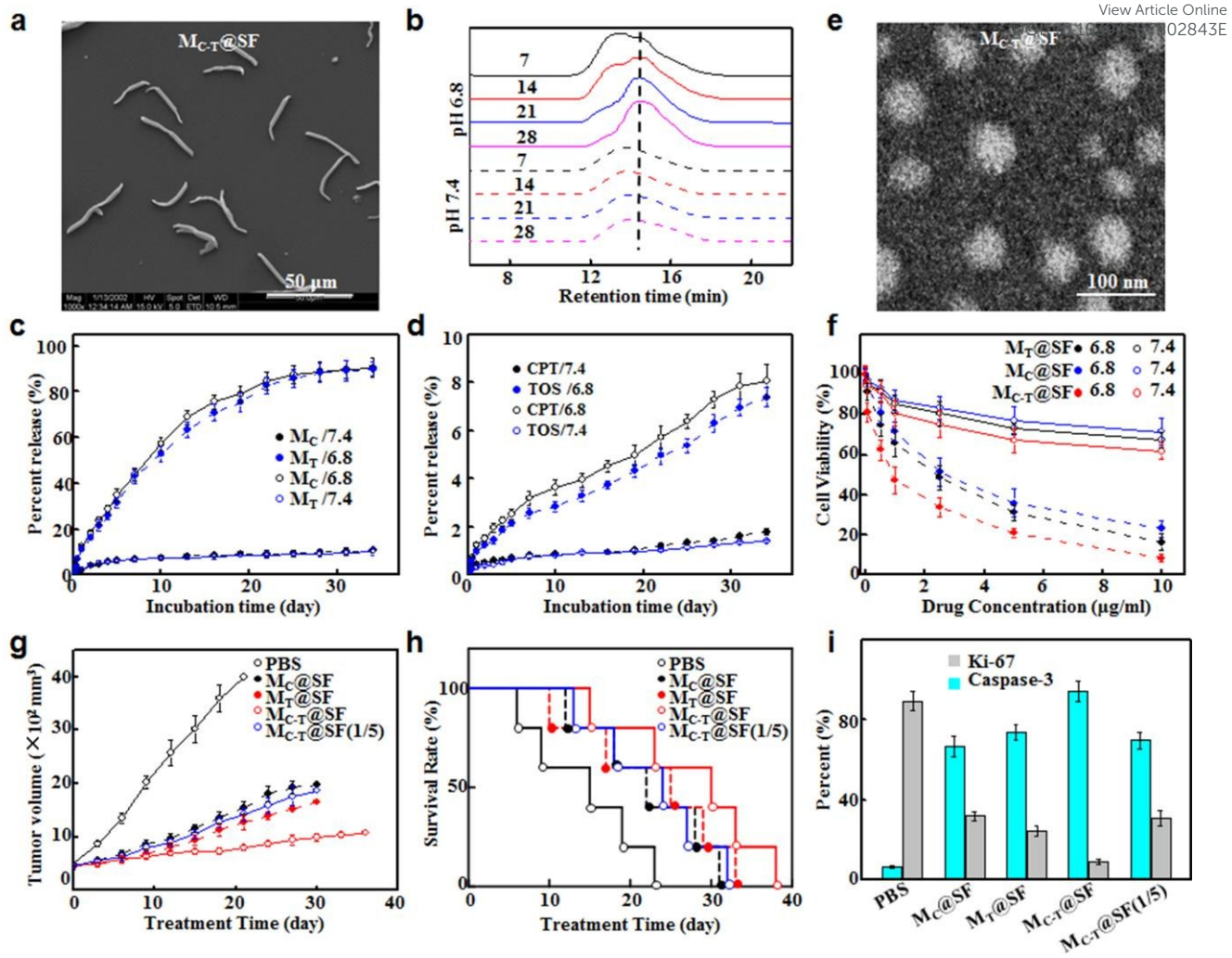

Fig. 5. Characterization of short fibers with loaded hybrid micelles. (a) SEM image of M_{C-T}@SF short fibers. (b) Typical GPC elution profiles of M_{C-T}@SF after incubation at 37 °C in pH 7.4 and 6.8 buffers for 7, 14, 21 and 28 days. (c) Percent release of micelles and (d) free drugs from M_{C-T}@SF after incubation in pH 7.4 and 6.8 buffers at 37 °C (n = 3). (e) Typical TEM images of M_{C-T} micelles released from M_{C-T}@SF. (f) Cytotoxicity to H22 cells after incubation for 72 h with M_C@SF, M_T@SF and M_{C-T}@SF in pH 7.4 and 6.8 media (n = 6). (g) Tumor growth, (h) overall survival of tumor-bearing mice, (i) the number of caspase-3 and Ki-67-positive cells compared with the total number of cells in IHC staining images of tumors retrieved on day 21 after intratumoral administration of M_C@SF, M_T@SF, M_{C-T}@SF and M_{C-T}@SF(1/5), using saline injection as control (n = 8).

around 90% of mass residual was detected after 4 weeks in pH 7.4. Fig. 5b shows GPC elution profiles of the retrieved M_{C-T}@SF during the degradation process. A shoulder peak appeared at the eluting time of 14.2 min (26 kDa) after incubation for 1 week in pH 6.8 buffers, and the shoulder peak gradually rose during the following weeks. There was almost no shoulder peaks after incubation in pH 7.4 buffers. It was indicated that HA-ss-CPT and HA-ss-TOS-TPP copolymers were released into the degradation media after the breakage of CDM linkers. As shown in the ^{1}H NMR spectrum, there were almost no characteristic peaks of HA after 4 weeks of incubation in pH 6.8 buffers (Fig. S10d).

3.8 Characterization of hybrid micelle release from short fibers

The acid-labile degradation of M_{C-T}@SF short fibers led to the release of amphiphilic copolymers of HA-ss-CPT and HA-ss-TOS-TPP. When both amphiphilic polymers were dispersed in an aqueous solution, hybrid micelles were formed with hydrophilic HA shells and hydrophobic cores of CPT and TOS-TPP.[20] Fig. 5c,d shows the percentage of micelles and free drugs released from M_{C-T}@SF after incubation in pH 7.4 and pH 6.8 buffers. Compared with around 10% of release in pH 7.4 buffers, around 90% of micelles were released from M_{C-T}@SF after 4 weeks of incubation in pH 6.8 buffers due to the acid-labile breakage of fiber matrix. As indicated above, the similar degradation profiles of M_C@SF and M_T@SF led to the simultaneous release of HA-ss-CPT and HA-ss-TOS-TPP. The polymer mixtures were self-assembled into M_{C-T} hybrid

micelles containing the same molar ratio of CPT and TOS-TPP as the blend ratio in the fiber matrix. There was less than 10% of drug release after incubation in pH 7.4 and pH 6.8 buffers for 4 weeks, due to the minimal hydrolysis of HA-ss-CPT and HA-ss-TOS-TPP (Fig. 5d). In addition, M_C@SF and M_T@SF showed similar release profiles of micelles (M_C and M_T) and free drug (CPT and TOS-TPP) to those of $M_{C\text{-}T}$@SF (Fig. S11a,b). Fig. 5e shows the typical TEM image of the retrieved $M_{C\text{-}T}$, indicating a spherical morphology with an average diameter of 57 nm. The retrieved M_C and M_T micelles had average sizes of 68 and 45 nm, which were close to those prepared *via* ultrasonication (Fig. S11c,d).

The reductive sensitivity of the retrieved micelles was determined with respect to the drug release and size changes in response to 10 μM, 10 and 40 mM of GSH. As shown in Fig. S11e,f the retrieved $M_{C\text{-}T}$ micelles had similar release profiles of CPT and TOS-TPP in response to the GSH levels. There was less than 10% of drug release after 96 h of incubation in PBS with or without 10 μM GSH, while over 85% of release in the presence of 10 and 40 mM of GSH. As shown in Fig. S11g, the incubation with 40 mM GSH led to a significant increase in $M_{C\text{-}T}$ size from 132 to 328 nm. In addition, there was no difference in the redox-responsive drug release and size change among the retrieved $M_{C\text{-}T}$, M_T and M_C micelles (Fig. S11h,i), which were also similar to those of fresh micelles prepared *via* ultrasonication (Fig. 2).

The cytotoxicities of micelles were determined on H22 cells after incubation with short fibers in pH 7.4 and 6.8 buffers. Fig. 5f shows the dose-dependent cytotoxicities of short fibers, indicating significantly higher cytotoxicities in pH 6.8 buffers than in pH 7.4. The IC_{50} values of M_C@SF, M_T@SF and $M_{C\text{-}T}$@SF in pH 6.8 buffers were expressed by the free drug concentrations and determined to be 1.41, 1.37, and 0.52 μg/mL, respectively, revealing the synergistic performance of hybrid micelles released from short fibers.

3.9 Antitumor efficacy after short fiber treatment

Fig. 5g summarizes the tumor growth in mice after treatment with M_C@SF, M_T@SF and $M_{C\text{-}T}$@SF. The tumors without treatment grew from around 500 to 3980 mm^3 after 21 days, and the treatment with M_T@SF and M_C@SF indicated around 68% and 61% of tumor growth inhibition, respectively. The most significant inhibition of tumor growth (80%) was detected for $M_{C\text{-}T}$@SF, reaching around 790 mm^3 in tumor volume after 21 days ($p < 0.05$). Moreover, the treatment with $M_{C\text{-}T}$@SF(1/5) showed considerable therapeutic effect comparable to those of M_T@SF and M_C@SF. The enhanced treatment efficacy of $M_{C\text{-}T}$@SF was also reflected in the survival rates of tumor-bearing mice (Fig. 5h), showing an extended median death time of 30 days. The treatments with M_T@SF,M_C@SF and $M_{C\text{-}T}$@SF(1/5) led to 50% dead mice after 25, 22, and 24 days, respectively.

Fig. S12a shows H&E staining images of tumors retrieved after treatment for 21 days. Intratumoral injection of short fibers led to obvious necrotic regions in tumors, and $M_{C\text{-}T}$@SF treatment showed the largest necrotic areas with overall pink staining. The cell proliferation and apoptosis in tumor tissues were evaluated by IHC staining of Ki-67 and caspase-3 (Fig. S12b,c), respectively, and Fig. 5i summarizes the percentage of positively stained cells. It was obvious that the $M_{C\text{-}T}$@SF treatment induced significantly higher cell apoptosis and lower proliferation compared with the other groups. There were around 94.2% of caspase-3-positive cells after $M_{C\text{-}T}$@SF treatment, which was more effective in apoptosis induction than M_C@SF and M_T@SF at around 66.8% and 73.6%, respectively ($p < 0.05$). Compared with around 32% (M_C@SF) and 24% (M_T@SF) of proliferative cells, the Ki-67-positive cells in tumors after $M_{C\text{-}T}$@SF treatment were around 9% ($p < 0.05$). In addition, the treatment with $M_{C\text{-}T}$@SF(1/5) led to around 69.6% and 30.9% of caspase-3 and ki-67-positive cells in tumors, respectively, indicating similar treatment efficacy to those of M_T@SF and M_C@SF.

Increase of tumor accumulation as well as co-loading and coordinate release of multiple drugs represent a challenging task for micelles to achieve a synergistic dose. To address these challenges, we confirmed the synergy effect of hybrid micelles, and then developed injectable short fibers as an implantable depot for micelle releasing to ensure the synergistic ratio of drugs in the targeting site. The acid-labile degradation of short fibers led to the release of HA conjugates, followed by self-assembly into hybrid micelles (Fig. 5). The blend ratio of PLA-cdm-M_C and PLA-cdm-M_T in short fibers defined the ratio of M_C to M_T in $M_{C\text{-}T}$ micelles. After HA-mediated cellular uptake, the cleavage of disulfide bonds resulted in effective and synchronous releases of TOS and CPT to maintain the synergistic drug ratio (Fig. 2). Next, we determined the combination index and dose-reduction index of hybrid micelles and confirmed the synergistic therapeutic efficacy with dose-reducing superiority. The 5-fold lower dose of $M_{C\text{-}T}$ produced higher ROS levels and induced similar cell apoptosis rates compared with M_C and M_T (Fig. 3). *In vivo* treatment with $M_{C\text{-}T}$(1/5) showed comparable tumor growth inhibition, slightly extended animal survival, and higher tumor necrosis than those of M_C and M_T (Fig. 4). It is worth to note that the dose reduction of $M_{C\text{-}T}$ significantly alleviated the side effect of drugs, indicating no hematologic and intestinal toxicities (Fig. S9). In addition, compared with M_T@SF and M_C@SF short fibers, the $M_{C\text{-}T}$@SF(1/5) treatment achieved similar antitumor profiles with respect to the tumor growth inhibition, animal survival, histological and IHC staining of tumor slices (Fig. 5g-i). Therefore, hybrid micelles or micelles-releasing short fibers with 5-fold reduced doses could maintain or increase the therapeutic efficacy while minimizing the side effects, offering high potential for synergistic cancer therapy.

4. Conclusions

Hybrid micelles are developed to coordinately release CPT and TOS for nucleus and mitochondrion interferences, followed by electrospinning into injectable short fibers for local tumor therapy. The synergistic effect of free CTP and TOS-TPP is confirmed, and the combination index and dose-reduction index of $M_{C\text{-}T}$ micelles are determined. Hybrid micelles

precisely deliver the drug combination at a synergistic ratio to the target site by simultaneous intracellular release of the combinations *via* synchronous disulfide cleavage, thus exhibiting significantly higher cytotoxicities. Compared with M_C and M_T micelles, $M_{C\text{-}T}$ with 5-fold lower doses produce higher intracellular ROS levels, comparable tumor growth inhibition and slightly higher animal survival, while indicating no hematologic and intestinal toxicities. The acid-labile degradation of $M_{C\text{-}T}$@SF short fibers leads to a sustained release of $M_{C\text{-}T}$ micelles with similar cellular uptake and cytotoxicity behaviors to those of micelles prepared *via* ultrasonication. $M_{C\text{-}T}$@SF with 5-fold lower doses achieve tumor growth inhibitions comparable to M_T@SF and M_C@SF and prolong animal survivals. Therefore, this study validates that the hybrid micelles or micelles-releasing short fibers could achieve enhanced therapeutic efficacy with dose-reducing superiority through drug synergy, highlighting their potential for synergistic chemotherapy.

Conflicts of interest

There are no conflicts of interest to declare.

Acknowledgements

This work was supported by National Natural Science Foundation of China (31771034 and 31470922), and the Key Research and Development Program of Sichuan Province (2018SZ0348).

Notes and references

1 Q. Hu, W. Sun, C. Wang and Z. Gu, *Adv. Drug Deliv. Rev.*, 2016, **98**, 19–34.
2 J. Kim, J. Kim, C. Jeong and W. J. Kim, *Adv. Drug Deliv. Rev.*, 2016, **98**, 99–112.
3 J. V. Natarajan, C. Nugraha, X. W. Ng and S. Venkatraman, *J. Control. Release*, 2014, **193**, 122–138.
4 S. Biswas, P. Kumari, P. M. Lakhani and B. Ghosh, *Eur. J. Pharm. Sci.*, 2016, **83**, 184–202.
5 M. O. Durymanov, A. A. Rosenkranz and A. S. Sobolev, *Theranostics*, 2015, **5**, 1007–1020.
6 H. Cho, T. C. Lai, K. Tomoda and G. S. Kwon, Polymeric micelles for multi-drug delivery in cancer, *AAPS PharmSciTech*, 2015, **16**, 10–20.
7 R. V. Kutty, C. Y. Tay, C. S. Lim, S. S. Feng and D. T. Leong, *Nano Res.*, 2015, **8**, 2533–2547.
8 L. Miao, S. Guo, C. M. Lin, Q. Liu and L. Huang, *Adv. Drug Deliv. Rev.*, 2017, **115**, 3–22.
9 M. Rui, Y. Xin, R. Li, Y. Ge, C. Feng and X. Xu, *Mol. Pharm.*, 2017, **14**, 107–123.
10 K. M. Camacho, S. Kumar, S. Menegatti, D. R. Vogus, A. C. Anselmo and S. Mitragotri, *J. Control. Release*, 2015, **210**, 198–207.
11 P. Parhi, C. Mohanty and S. K. Sahoo, *Drug Discov. Today*, 2012, **17**, 1044–1052.
12 O. Naksuriya, S. Okonogi, R. M. Schiffelers, W. E. Hennink, *Biomaterials*, 2014, **35**, 3365–3383.
13 J. R. Weiser and W. M. Saltzman, *J. Control. Release*, 2014, **190**, 664–673.
14 R. R. Thakur, H. L. McMillan and D. S. Jones, *J. Control. Release*, 2014, **176**, 8–23.
15 A. J. Meinel, O. Germershaus, T. Luhmann, H. P. Merkle and L. Meinel, *Eur. J. Pharm. Biopharm.*, 2012, **81**, 1–13.
16 Z. Chen, W. Liu, L. Zhao, S. Xie, M. Chen, T. Wang and X. Li, *Biomacromolecules*, 2018, **19**, 1100–1110.
17 L. Milane, M. Trivedi, A. Singh, M. Talekar and M. Amiji, *J. Control. Release*, 2015, **207**, 40–58.
18 L. Wang and C. Li, *J. Mater. Chem.* 2011, **21**, 15862–15871.
19 G. Saito, J. A. Swanson and K. D. Lee, *Adv. Drug Deliv. Rev.*, 2003, **55**, 199–215.
20 L. Qiu, M. Qiao, Q. Chen, C. Tian, M. Long, M. Wang, Z. Li, W. Hu, G. Li, L. Cheng, L. Cheng, H. Hu, X. Zhao and D. Chen, *Biomaterials*, 2014, **35**, 9877–9887.
21 Z. Chen, N. He, M. Chen, L. Zhao and X. Li, *Acta Biomater.*, 2016, **43**, 195–207.
22 H. Therien-Aubin, Y. Wang, K. Nothdurft, E. Prince, S. Cho and E. Kumacheva, *Biomacromolecules*, 2016, **17**, 3244–3251.
23 G. P. Kalemkerian and X. L. Ou, *Cancer Chemother. Pharmacol.*, 1999, **43**, 145–150.
24 Y. F. Brun, C. G. Dennis, W. R. Greco, R. J. Bernacki P. J. Pera, J. J. Bushey, C. Y. Richard, D. B. White and B. H. Segal, *Antimicrob. Agents Chemother.*, 2007, **51**, 1804–1812.
25 W. Scarano, P. de Souza and M. H. Stenzel, *Biomater. Sci.*, 2015, **3**, 163–174.
26 X. Luo, G. Xu, H. Song, S. Yang, S. Yan, G. Jia and X. Li, *Eur. J. Pharm. Biopharm.*, 2012, **82**, 545–553.
27 A. Angulo-Molina, J. Reyes-Leyva, A. Lopez-Malo and J. Hernandez, *Nutr. Cancer*, 2014, **66**, 167–176.
28 D. Liang, A. T. Wang, Z. Z. Yang, Y. J. Liu and X. R. Qi, *Mol. Pharm.*, 2015, **12**, 2189–2202.
29 M. Chen, Y. Zhang, Z. Chen, S. Xie, X. Luo and X. Li, *Acta Biomater.*, 2017, 49, 444–455.
30 V. Gogvadze, S. Orrenius and B. Zhivotovsky, *Trends Cell Biol.*, 2008, **18**, 165–173.
31 T. C. Chou, *Cancer Res.*, 2010, **70**, 440–446.
32 F. Ewald, D. Norz, A. Grottke, B. T. Hofmann, B. Nashan and M. Jucker, *Invest. New Drugs*, 2014, **32**, 1144–1154.
33 B. Deng, M. X. Xia, J. Qian, R. li, L. J. Li, J. L. Shen, G. W. Li, Y. Xie, *Mol. Pharm.*, 2017, **14**, 1938-1949.
34 X. M. Luo, M. H. Chen, Y. Zhang, Z. J. Chen and X. H. Li, *Eur. J. Pharm. Biopharm.*, 2016, **98**, 9-19.
35 T. Nakaoka, A. Ota, T. Ono, S. Karnan, H. Konishi, A. Furuhashi, Y. Ohmura, Y. Yamada, Y. Hosokawa and Y. Kazaoka, *Cell. Oncol.*, 2014, **37**, 119–129.
36 H. Lee, C. H. Ahn and T. G. Park, *Biosci.*, 2009, **9**, 336–342.
37 S. J. Ralph, S. Rodriguez-Enriquez, J. Neuzil and R. Moreno-Sanchez, *Mol. Aspects Med.*, 2010, **31**, 29–59.
38 N. Sen, B. B. Das, A. Ganguly, T. Mukherjee, G. Tripathi, S. Bandyopadhyay, S. Rakshit, T. Sen and H. K. Majumder, *Cell Death Differ.*, 2004, **11**, 924–936.
39 L. F. Dong, V. J. Jameson, D. Tilly, J. Cerny, E. Mahdavian and A. Marin-Hernandez, et al., *J. Biol. Chem.*, 2011, **286**, 3717–3728.
40 K. N. Ogston, I. D. Miller, S. Payne, A. W. Hutcheon, T. K. Sarkar and I. Smith, et al., *The Breast*, 2003, **12**, 320–327.
41 A. Urruticoechea, I. E. Smith, M. Dowsett, *J. Clin. Oncol.*, 2005, **23**, 7212–7220.
42 A. Rodriguez-Hernandez, G. Brea-Calvo, D. J. Fernandez-Ayala, M. Cordero, P. Navas and J. A. Sanchez-Alcazar, *Apoptosis*, 2006, **11**, 131–139.
43 U. Swami, S. Goel and S. Mani, *Curr. Drug Targetes*, 2013, **14**, 777–797.
44 C. Y. Sun, S. Shen, C. F. Xu, H. J. Li, Y. Liu and Z. T. Cao, et al., *J. Am. Chem. Soc.*, 2015, **137**, 15217–15224.

View Article Online
DOI: 10.1039/C8TB02843E